Polar Research

Late Jurassic/Early Cretaceous phosphates of Nordvik, North Siberian Basin

Henning Dypvik[1] & Victor Zakharov[2]

1 Department of Geosciences, University of Oslo, PO Box 1047, Blindern, NO-0316 Oslo, Norway
2 Geological Institute, Russian Academy of Sciences, Pyzhevskij 7, RU-109017 Moscow, Russia

Keywords
Geochemistry; Jurassic/Cretaceous; phosphates; sedimentology; Siberia.

Correspondence
Henning Dypvik, Department of Geosciences, University of Oslo, PO Box 1047, Blindern, NO-0316 Oslo, Norway. E-mail: henning.dypvik@geo.uio.no

doi:10.1111/j.1751-8369.2010.00171.x

Abstract

Late Jurassic and Early Cretaceous calcite-rich phosphate (fluor/hydroxy apatite) concretions in the North Siberian basin (Nordvik) have been analysed. Their mineralogical and geochemical (major, trace and rare earth element) characteristics are presented in a sedimentological context. Low oxygen conditions prevailed along large parts of the seafloor of this wide epicontinental sea. In the Nordvik region this, in combination with slow and very fine-grained clastic sedimentation, and high algal production, resulted in the formation of phosphatic concretions. The concretions mainly consist of microcrystalline to ultracrystalline apatite and calcite, with traces of sphalerite, pyrite, kaolinite, quartz and albite. The clastic composition of the concretions is comparable with the surrounding Nordvik shales. Dysoxic–anoxic conditions in the last precipitating pore-water phases (early diagenetic) are reflected in enrichments in, for example, vanadium, uranium and the rare earth elements in the concretions.

An extensive Late Jurassic epicontinental basin covered large parts of the present Arctic Basin (Fig. 1). In this study mineralogical and geochemical analyses of calcite-rich phosphate concretionary beds from field sections in the Nordvik area (North Siberian Basin) are presented. The aim was to describe and better explain the phosphate formation, and to search for possible geochemical signals of the Late Jurassic Mjølnir impact (Dypvik et al. 1996). Zakharov et al. (1993) described large iridium anomalies from one of these beds, and therefore this bed (NV18/NV18a/NV18b) and the surrounding beds were re-sampled and analysed in great detail.

Geological background information

In the Nordvik region of the North Siberian Basin, Volgian and Lower Valanginian deposits constitute the Paksa Formation (Figs. 1, 2), which is composed of alternating dark-grey and brown mudstones and bluish-grey massive claystones/shales, with numerous interbeds of phosphate/carbonate concretions (Fig. 3). The Jurassic to Cretaceous stratigraphical successions can be fairly well correlated in the Arctic area, e.g., between North Greenland, Svalbard and the Barents Sea (Fig. 2). The total thickness of the Paksa Formation is 137.5 m.

The concretionary beds are exposed in tilted coastal cliffs, and in the field can be followed for tens of metres. The layers consist of elongated concretionary lenses, 10–25 cm long and 3–15 cm thick, appearing in well-defined, more or less continuous layers (Figs. 2–4). Several concretionary units can be found within these laminated, black shales, normally from 50–150 cm apart. The concretions are light brown, orange to brown, or almost black in colour. They may contain some dark zones, occurring in parallel with and in a few cases across the common, fine lamination (Fig. 4). The concretions show a pristine appearance along the lamination, without any signs of secondary reworking. The very fine, parallel lamination shows faint undulations, without swelling or pinching.

Samples and methods

Forty-two samples from seven concretions (calcite-rich phosphate) (NV16, NV1740, NV18, NVa18, NVb18, NV19 and NV33/17) from the 18-m-thick section of the Paksa Formation of Nordvik (Siberia) have been analysed, in addition to four typical shales from the formation (Figs. 2–4). The concretions were split (into between 3 and 10 slices), as indcated by the labelling within bed NV18 (Fig. 4). Centimetre-thick slices of phosphatic concretions were cut for detailed geochemical analysis in our search for traces of the Mjølnir impact event (Zakharov

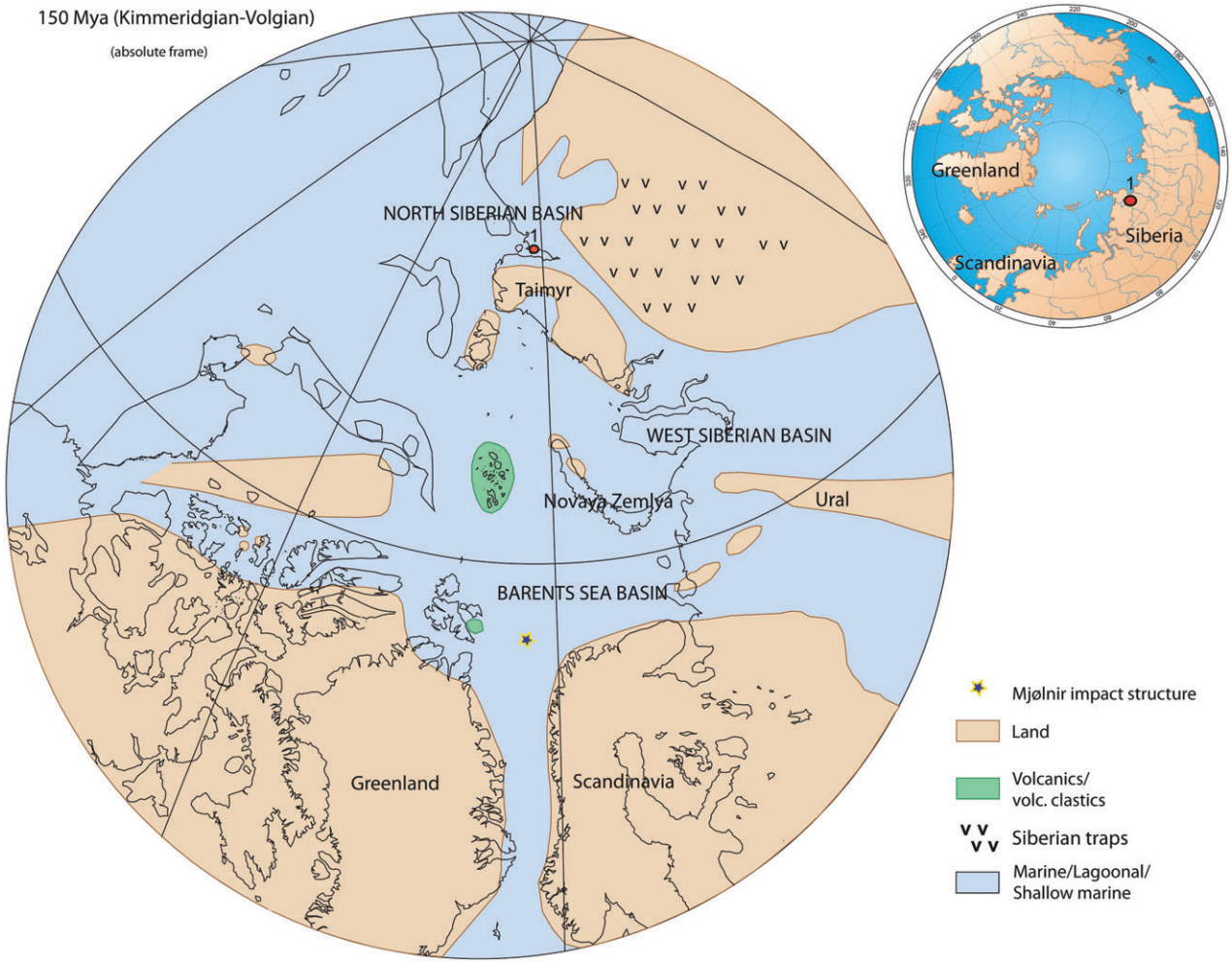

Fig. 1 This representation of the simplified late Jurassic palaeogeography of the Arctic is based on the plate reconstructions of Lawver et al. (1990).

et al. 1993; Dypvik et al. 1996). The shales and phosphates were studied in thin section and using scanning electron microscopy (SEM), before being crushed and analysed using X-ray diffraction (XRD) and inductively coupled plasma (ICP) mass spectroscopy (MS).

The XRD analyses were executed on rock powder samples (randomly oriented, pressed pellets of crushed rock powder) on an X'Pert system (Philips Analytical [now Panalytical], Almelo, the Netherlands) at the University of Oslo, with detection limits of about 5%. The values presented in Table 1 are semi-quantitative XRD % values, calculated from the peak area of the main peaks in the X-ray diffractograms. They should not be confused with real concentrations; the relative compositional variations, however, are well depicted in the data. The clay mineralogical analyses were performed according to the standard methods of Carroll (1970): untreated, ethylene glycolation, heating to 550°C and slow scan across the 3.55-Å area.

The geochemical analyses were performed at Activation Laboratories (ActLab, Ancaster, Ontario, Canada) using element fusion (ICP-MS, ActLab code 4LITHO), major elements fusion ICP (ActLab code WRA) and trace elements fusion ICP/MS (ActLab code WRA4B2) (Tables 1–4). In these analyses the detection limits were as given in Table 2.

In the rare earth element (REE) analysis the concentrations have been normalized to general upper continental crust values (Condie 1991). This was done for comparison with the clastic claystones and shales, which represent fairly well mixed continental weathering products from a wide area; consequently, a continental crust composition forms a reasonable base for comparison.

The total organic carbon (TOC) concentrations were determined by a standard combustion technique (CR-412 multi-carbon analyser, Leco, St. Joseph, MI, USA) at the Department of Geosciences, University of Oslo (Table 1), with a precision of ±1%.

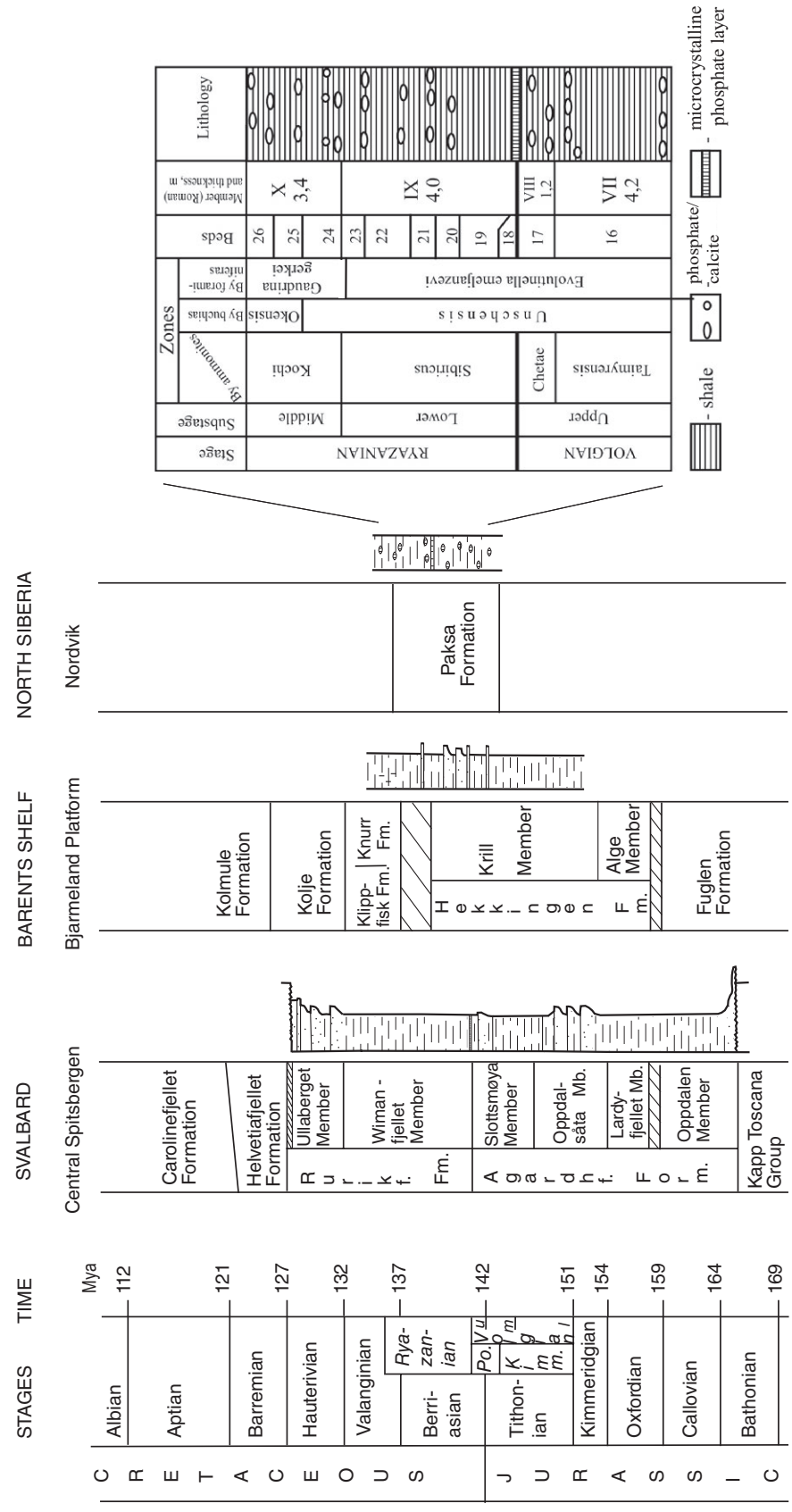

Fig. 2 Comparison of Svalbard, Barents Sea and Nordvik stratigraphy. General lithological information is presented in standard signatures; Po, Portlandian (based on Dypvik et al. [2002]). The detailed stratigraphical section of the Jurassic–Cretaceous boundary beds of the Paksa Formation at the Nordvik peninsula (Urdyuk-Khaya Cape), Laptev Sea, are shown in the right-hand column.

Fig. 3 Photograph of the studied section at Nordvik, showing the common appearance of black shales and phosphatic/carbonate concretionary beds.

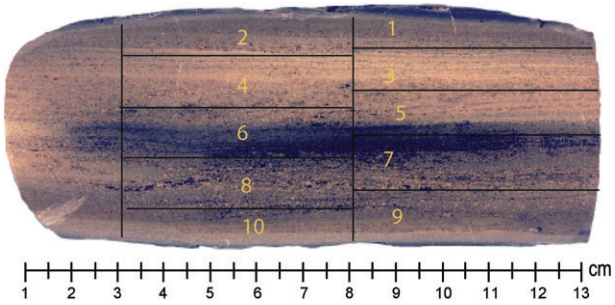

Fig. 4 A calcite-rich phosphate concretion from Nordvik, sample NV18. The sample split and numbering nomenclature are indicated in the photograph. Fine lamination is well developed, and the central part displays dark-grey staining.

In this study instrumental neutron activation analysis of samples from Nordvik beds revealed that they display only weak iridium concentrations—a maximum of about 200 ppt (F.T. Kyte, pers. comm.)—and these results will not be discussed any further.

Results and discussion

Mineralogy

The analysed Nordvik shales are very fine-grained, well-laminated and contain pellets and a few dispersed grains of glauconite. They are poor in coarser grains, for example, of quartz and feldspar, compared with the shales analysed from the western Arctic (North Greenland, Svalbard and the Barents Sea). In the black shale succession of the Nordvik section, more or less continuous concretionary beds, 5–12 cm in thickness, of phosphates and carbonates are present (Figs. 2, 3). In the concretions fine-grained, microcrystalline and ultracrystalline apatite and calcite dominate, with numerous fossil fragments of foraminiferas (e.g., *Ammobaculites* and *Lenticulina*), ostracodes (e.g., *Bairdia*), calcispheres, radiolarians, bryozoans, possible algal filaments and even large pieces of bone. The fossil fragments make up to 30% of the concretions, whereas they only form 1–2% of the shales (Figs. 5, 6). In the phosphate concretions sphalerite (ZnS), pyrite (FeS_2) and a very few grains of quartz and albite, as well as possible illite, chlorite and kaolinite fragments, have been detected in the dense, microcrystalline apatite and micritic calcite cement. Generally the calcite is well distributed throughout the concretionary phosphates, but faint calcite enrichments may be present in various parts of the concretions. The quantities of quartz, feldspar, mica and albite increase towards their outer rims. This is seen in the thin sections but is difficult to trace in hand-sized pieces. The major parts of pyrite are found to be dispersed as framboidal crystals of possible late diagenetic origin. Organic matter, such as fragments of palynomorphs, make up large parts of the TOC, giving the concretions an overall brownish colour. The Paksa Formation shales have TOC contents, in the Middle Volgian through Middle Ryazanian/Berriasian interval, varying from 1.0–3.5%. The TOC values drop to an average of about 0.5% in the siltier Upper Ryazanian/Berriasian and Lower Valanginian beds. Within the different concretions the mineralogical variations are minor. The seven concretions studied have related and comparable mineralogical and geochemical compositions (Tables 1, 3–5). The X-ray diffraction analyses (Table 1) show that apatite and calcite dominate the phosphate concretions, with only sparse quantities of silicates and pyrite present.

Geochemistry: correlations

The concretions display correlation coefficients related mainly to three populations: a clastic/silicate, a carbonate and a phosphate fraction. The silicate fraction (with the total quantity of silicates estimated from XRD analysis) is positively correlated with the SiO_2, K_2O, TiO_2, V, Cr, Tb, Cs, Hf, REEs, Th, U, Sc, Y, Nb and partly MgO and Fe_2O_3 concentrations. The calcite fraction (with calcite quantities based on XRD analysis) is negatively correlated with most major (except MnO and CaO) and trace elements. The apatite fraction (apatite quantities based on XRD analysis) does not show positive correlations with any of the elements, and is negatively correlated with calcite. The large quantities of apatite and calcite have, consequently, caused severe internal dilution effects on the detrital, clastic mineral phases, which seem to carry most trace element variations (Table 1). The generally very poor geochemical correlations achieved may be the result

Table 1 X-ray diffraction analyses (silicates, calcite, apatite and pyrite) and main element geochemistry of phosphate/carbonate concretions and four typical shales from the Nordvik section.

Nordvik	Silicates %	Calcite %	Apatite %	Pyrite %	SiO_2 %	Al_2O_3 %	Fe_2O_3 %	MnO %	MgO %	CaO %	Na_2O %	K_2O %	TiO_2 %	P_2O_5 %	LOI %	Total %	TOC %
NV19-1	4	5	90	1	7.13	2.74	3.03	0.138	0.76	43.48	1.35	0.39	0.131	28.79	10.87	98.81	1.77
NV19-2	5	9	85	1	6.57	2.19	6.67	0.166	1.11	41.51	1.09	0.32	0.107	27.20	12.70	99.63	1.78
NV19-3	5	11	83	1	7.88	2.69	17.91	0.284	2.15	30.49	0.76	0.34	0.106	18.48	17.57	98.66	2.26
NV19-4	4	10	85	1	5.76	1.95	3.53	0.132	0.80	44.16	1.14	0.34	0.104	29.76	10.97	98.65	1.80
NV19-5	4	12	83	1	5.83	2.04	3.86	0.146	0.80	43.92	1.24	0.32	0.102	29.69	11.02	98.97	1.62
NV16-1	6	26	67	1	8.35	3.12	3.59	0.174	0.75	42.67	1.20	0.40	0.152	23.69	14.91	99.01	1.78
NV16-2	4	17	78	1	3.56	17.30	2.34	0.133	0.44	39.67	1.04	0.21	0.081	24.68	9.51	98.96	1.19
NV16-3	2	18	79	1	3.31	1.29	2.38	0.187	0.40	47.82	1.12	0.20	0.075	28.81	13.00	98.59	1.62
NV16-4	4	25	70	1	3.53	1.34	2.46	0.178	0.41	48.35	1.08	0.16	0.072	28.97	13.19	99.74	1.67
NV16-5	4	39	56	1	7.53	2.77	3.61	0.194	0.74	44.07	0.97	0.35	0.140	21.16	17.53	99.06	1.49
NV1740-1	5	30	63	2	7.39	3.00	3.71	0.183	0.80	43.74	1.04	0.31	0.164	23.38	15.41	99.13	2.16
NV1740-2	2	26	71	1	3.12	1.28	2.38	0.169	0.50	48.98	1.10	0.08	0.086	28.91	12.81	99.42	1.66
NV1740-3	2	33	64	1	3.23	1.36	2.49	0.211	0.56	48.59	0.95	0.16	0.079	26.06	15.30	98.99	1.36
NV1740-4	2	41	56	1	2.95	1.22	2.56	0.230	0.55	48.62	0.90	0.10	0.067	24.78	16.64	98.62	1.29
NV1740-5	3	22	74	1	3.96	1.64	2.59	0.178	0.57	47.05	1.10	0.23	0.099	28.65	12.77	98.84	2.02
NV33/17	8	17	74	1	10.10	3.80	3.37	0.138	0.80	41.18	1.13	0.53	0.190	25.84	11.51	98.59	1.51
NVa18-1	4	42	53	1	7.63	2.80	4.27	0.181	0.77	43.63	0.89	0.36	0.145	19.22	19.13	99.03	1.58
NVa18-2	4	46	49	1	7.32	2.70	4.30	0.189	0.77	43.94	0.83	0.33	0.139	18.40	20.13	99.05	1.43
NVa18-3	3	22	74	1	4.48	1.67	2.62	0.132	0.43	47.99	1.02	0.24	0.091	28.79	11.98	99.44	1.35
NVa18-4	3	29	67	1	4.53	1.69	3.66	0.144	0.46	47.74	1.01	0.24	0.095	26.90	13.28	99.75	1.27
NVa18-5	2	27	70	1	2.92	1.17	2.74	0.144	0.40	49.22	1.00	0.19	0.059	28.26	12.83	98.93	1.44
NVa18-6	2	27	70	1	2.93	1.15	2.73	0.145	0.40	49.85	1.01	0.14	0.058	28.31	13.20	99.92	1.41
NVa18-7	2	21	76	1	3.32	1.29	1.96	0.146	0.35	49.02	1.10	0.15	0.072	28.97	12.49	98.87	1.50
NVa18-8	2	23	74	1	3.06	1.19	2.73	0.150	0.35	48.90	1.09	0.20	0.068	29.33	11.91	98.98	1.55
NVa18-9	8	22	69	1	7.98	2.95	3.83	0.141	0.60	42.80	1.19	0.41	0.155	25.35	13.30	98.71	1.92
NVa18-10	5	24	70	1	7.01	2.61	3.35	0.142	0.55	44.54	1.21	0.35	0.139	26.24	13.10	99.24	1.75
Nvb18-1	5	30	64	1	6.95	2.56	3.33	0.181	0.70	44.72	1.16	0.33	0.140	23.97	14.83	98.87	1.82
Nvb18-2	4	30	65	1	7.44	2.74	3.65	0.185	0.75	43.63	1.24	0.34	0.149	23.86	15.05	99.03	1.82
NVb18-3	3	29	67	1	4.61	1.69	2.64	0.182	0.53	46.95	1.11	0.22	0.108	26.38	14.49	98.91	1.67
NVb18-4	2	28	69	1	4.33	1.59	2.63	0.178	0.52	47.13	1.18	0.21	0.103	26.95	13.81	98.63	1.55
NVb18-5	6	48	45	1	10.00	3.60	4.58	0.217	0.99	40.79	0.95	0.44	0.185	16.94	20.23	98.92	1.45
NVb18-6	6	47	46	1	9.82	3.51	4.69	0.214	1.00	41.17	1.01	0.42	0.180	16.98	20.07	99.06	1.45
NV18-1	7	28	64	1	8.77	4.55	3.89	0.155	0.69	41.71	1.15	0.39	0.169	22.50	15.23	99.2	1.85
NV18-2	8	34	56	2	11.64	4.27	4.89	0.164	0.88	39.49	1.11	0.51	0.212	18.84	17.18	99.19	2.10
NV18-3	2	19	78	1	3.32	1.31	2.58	0.142	0.33	48.97	1.17	0.21	0.075	30.12	11.23	99.46	1.70
NV18-4	3	21	75	1	3.77	1.46	2.29	0.144	0.35	48.26	1.21	0.21	0.088	29.71	12.42	99.91	1.65
NV18-5	3	21	75	1	4.25	1.86	2.84	0.138	0.41	47.71	1.15	0.21	0.087	29.14	11.18	98.98	1.42
NV18-6	6	68	24	2	3.84	1.51	2.98	0.145	0.38	47.55	1.12	0.25	0.084	29.38	11.51	98.75	1.48
NV18-7	3	22	74	1	3.54	1.32	2.46	0.139	0.37	48.65	1.02	0.18	0.082	29.07	12.21	99.04	1.36
NV18-8	3	30	66	1	4.23	1.64	2.83	0.150	0.45	48.36	0.98	0.24	0.092	26.83	14.05	99.85	1.29
NV18-9	5	40	54	1	7.22	2.68	4.22	0.175	0.71	43.78	0.92	0.32	0.143	20.62	18.02	98.81	1.57
NV18-10	7	41	50	2	11.35	4.19	6.87	0.180	1.11	38.52	0.93	0.53	0.219	15.72	19.43	99.05	1.91
Shales																	
NV0.25	93	2	0	5	48.62	18.50	9.30	0.03	2.45	1.07	1.65	2.53	1.09	0.35	13.54	99.13	3.64
NV12.10	91	1	0	8	46.32	16.02	12.68	0.03	2.52	0.51	1.27	2.58	0.82	0.18	16.15	99.07	3.49
NV12.60	84	0	0	16	54.36	18.81	7.32	0.03	2.96	0.33	1.41	3.03	1.07	0.11	9.94	99.36	0.99
NV13.20	91	4	0	5	24.73	8.49	29.76	0.31	5.72	2.66	0.71	1.44	0.42	0.23	24.6	99.06	3.72

of the coarse semi-quantitative XRD methods used in establishing the mineral fractions. The established geochemical element associations (correlation coefficient analysis) are as follows. Association 1 comprises SiO_2, MgO, K_2O, TiO_2, Y, Zr, Cr, Rb, Nb, Cs, Hf, Th, U and REEs. Association 2 comprises Fe_2O_3, MgO and Pb. Association 3 comprises CaO, P_2O_5, Ba and Sr, and is negatively correlated with K_2O, SiO_2, TiO_2, Y, V, Zr, Cr, Rb, Nb, Cs, Hf, U, Th, REEs, Na_2O and Be. Association 3 reflects the carbonate/phosphate association, which was not fully

Table 2 Detection limits for main and trace elements of phosphate and shale analysis. Values from ActLab, Ancaster, Ontario.

Main elements	Detection limit
SiO_2, Al_2O_3, Fe_2O_3, MgO, CaO	0.01 %
Na_2O, K_2O, P_2O_5, LOI (loss of ignition)	0.01 %
MnO, TiO_2	0.001 %
Trace elements	
Sc, Be, Co, Ga	1 ppm
Sr, Y, Rb	2 ppm
Ba	3 ppm
Zr	4 ppm
V, As	5 ppm
Cu	10 ppm
Cr, Ni	20 ppm
Zn	30 ppm
Rare earth elements	
La, Ce, Nd, Sm, Gd, Tb, Dy, Ho, Er, Yb	0.1 ppm
Lu	0.04 ppm
Pr, Eu, Tm	0.05 ppm

discovered in the XRD-quantified mineral–trace element correlations. Tables of correlation coefficients can be obtained by contacting the first author.

Geochemistry: Siberia shale and phosphates

Nordvik shales and phosphate concretion compositional comparison. In thin section and by XRD analyses the fine-grained and well-laminated Nordvik shales are seen to be rich in clay minerals (smectites, chlorite, mixed-layer illite smectite, kaolinite and illite), mica, quartz and plagioclase, and to have minor quantities of calcite and pyrite. In contrast, the concretions mainly consist of microcrystalline to ultracrystalline apatite, but some calcite and traces of spalerite, pyrite, organic material, kaolinite, quartz, mica and albite are also found. Dolomite has not been detected. Subtle calcite enrichments may be found in the central parts of the concretions, whereas the quantities of quartz, feldspar, mica and albite increase towards the rims. The XRD analyses show the clastic components of the apatite concretions to be comparable with the Nordvik shales in composition, as reflected in their main and trace-element compositions, e.g., comparable SiO_2, MnO, MgO, K_2O and TiO_2 distributions related to Al_2O_3 (element/Al_2O_3 ratios) in both shales and phosphates (Tables 1, 5). However, there are major differences in geochemical composition between shales and phosphates, with enrichments of CaO, Fe_2O_3, Na_2O, P_2O_5, Ba, Sr, U, V and TOC in the phosphates compared with the shales, which in turn are enriched in the main siliciclastic components (e.g., SiO_2, Al_2O_3, TiO_2 and K_2O) and associated trace elements (Zr, Cr, Co, Ni, Zn, Ga, As, Rb, Nb, Sb, Cs, Hf, Pb and Th). The yttrium, copper and molybdenum distributions vary, whereas scandium, beryllium, tantalum and thallium are found in about equal quantities in the concretions and shale samples analysed (Tables 1, 3, 4).

According to the XRD analyses the apatite is most likely to be fluor or hydroxy apatite. Compared with the studies of McClellan & Lehr (1969) and Guldbrandsen (1970), it may carry the XRD characteristics of hydroxy apatite. The comparable Triassic phosphate concretions of Svalbard have similar concentrations of P_2O_5 (3–26%) and TOC (1–8%), and are generally composed of carbonate fluorapatite (Krajewski 2000a, b, c).

The analysed Nordvik shales (containing 213 ppm REEs on average) normally have higher REE concentrations than the central parts of the phosphates (Table 4). In the phosphate concretions, however, internal variations are detected in the REE distributions. The outer rims have the highest total REE quantities, much higher than the surrounding shales. The shales display somewhat higher thorium/uranium ratios and zinc concentrations than the phosphates. The shales also have different REE distribution patterns than, for example, the heavy rare earth element (HREE)-enriched outer rims of the concretions (Fig. 7). (HREEs are Dy, Ho, Er, Tm, Yb and Lu.)

Trace element variations within phosphates and shales. The trace element composition in the different concretions studied is rather similar and independent of the stratigraphical level. Most trace element concentrations are comparable in the different concretions (Table 3). The arsenic, nickel, chromium and cobalt distributions vary, whereas the rims of the concretions are enriched in zinc, vanadium, uranium and REEs, and sometimes ytrium and molybdenum. The concretionary REE variations commonly show low total REE concentrations in their central parts, compared with the rim, where large total REE enrichments may occur. The light rare earth element (LREE: La, Ce, Pr and Nd)/HREE ratios, however, are constant throughout the concretions (Table 4).

Within the phosphates a few key ratios (Sc/Al_2O_3, K_2O/Al_2O_3, Ba/Al_2O_3, Cu/Al_2O_3, Zn/Al_2O_3, V/Cr and TOC/Al_2O_3) have been picked out in order to illustrate possible changes in the clastic components. The variations are small, reflecting only moderate compositional differences in their clastic content (Table 5). The Cu/Al_2O_3 and Zn/Al_2O_3 ratios are without any zonation in most concretions. They are, however, low in the central parts of a few concretions (Table 5).

The elemental ratios of V/Cr, V/Cu, Cr/Cu, Mo/Cu, Mo/Zn, Cu/Zn and Th/U in the concretions display values

Table 3 Results of trace element analyses of phosphates and four typical shales from the Nordvik section.

	Sc ppm	Be ppm	V ppm	Ba ppm	Sr ppm	Y ppm	Zr ppm	Cr ppm	Co ppm	Ni ppm	Cu ppm	Zn ppm	Ga ppm	As ppm	Rb ppm	Nb ppm	Mo ppm	Sb ppm	Cs ppm	Hf ppm	Ta ppm	Tl ppm	Pb ppm	Th ppm	U ppm
Nordvik																									
NV19-1	19	5	145	3340	4470	200	50	40	0	0	24	91	5	9	16	2	0	0	1.2	1	0.1	0.1	0	1.6	12.2
NV19-2	12	4	141	3140	4490	37	45	30	0	0	19	38	3	11	13	2	0	0	0.9	0.7	0.2	0.1	0	1.3	4
NV19-3	9	3	231	1680	2260	31	35	34	0	0	14	0	4	12	14	2	0	0.7	1	0.6	0.1	0.1	8	1.2	2
NV19-4	11	5	120	3810	5650	37	45	32	0	0	17	62	3	6	13	2	0	0.8	0.9	0.7	0.1	0	0	1.3	4.3
NV19-5	6	5	115	3220	4890	26	37	30	0	0	21	87	3	7	13	2	2	0	0.9	0.7	0.2	0.1	0	1.3	6.8
NV16-1	37	5	190	2290	3260	354	59	34	0	22	16	93	5	5	15	2	15	0	0.9	0.9	0	0.3	0	1.6	24.3
NV16-2	6	4	84	2600	3540	27	37	23	0	23	12	31	17	11	8	1	8	0.8	0.6	0.6	0.1	0.2	0	0.9	7.4
NV16-3	4	4	81	2850	3830	8	34	0	0	0	11	46	2	10	8	1	9	0.6	0.6	0.5	0.1	0.3	0	0.8	4.2
NV16-4	9	4	88	2740	3870	36	38	0	0	30	12	67	2	0	8	1	9	0	0.7	0.5	0.1	0.3	0	0.8	3.3
NV16-5	26	4	187	2030	3110	193	75	36	0	26	15	122	3	6	15	2	14	0.5	1	1.1	0	0.3	0	1.4	15.6
NV1740-1	62	5	243	2070	3170	489	79	42	2	30	24	561	5	9	12	2	12	0.9	0.9	1.4	0	0.5	0	1.3	40.1
NV1740-2	20	4	145	2760	3810	127	42	22	0	0	13	155	2	8	6	2	9	0.7	0	0.6	0	0.2	0	2.1	10.3
NV1740-3	7	4	138	2270	3470	14	34	0	0	23	13	52	3	0	7	1	6	0	0	0.5	0.1	0.2	0	0.7	3.3
NV1740-4	5	3	136	2130	3400	9	34	0	0	0	15	80	2	0	4	1	7	0	0	0.5	0.1	0.2	0	0.6	2.5
NV1740-5	33	5	158	2590	3630	251	48	27	0	21	14	376	3	0	6	2	8	0	0.5	0.9	0	0.3	0	0.8	14.1
NV33/17	35	4	217	2360	3490	300	74	51	0	0	21	127	6	16	23	3	4	0	1.6	1.4	0.1	0.2	0	2.3	16.2
NVa18-1	28	3	181	1740	3120	208	72	45	0	32	15	77	4	7	14	2	20	0	0.9	1.3	0	0.3	0	1.5	20.7
NVa18-2	29	3	184	1880	3170	226	75	44	0	35	16	185	5	8	15	2	19	0.6	1	1.2	0	0.4	0	1.4	20.3
NVa18-3	7	3	87	2520	3800	18	34	24	0	0	12	46	3	5	13	1	9	0	0.8	0.6	0.1	0.3	0	1.1	2.3
NVa18-4	12	4	98	2250	3620	42	40	26	0	24	0	94	3	0	11	1	12	0	0.7	0.6	0.1	0.3	0	1	2.7
NVa18-5	3	3	79	1700	3990	5	21	0	0	0	0	0	2	15	7	1	10	0.6	0	0.4	0.1	0.2	0	0.7	2.9
NVa18-6	3	3	75	2590	3730	4	22	0	0	21	10	59	2	13	8	1	10	0.6	0.5	0.4	0.1	0.4	0	0.7	2
NVa18-7	5	4	95	2870	4170	14	32	23	0	22	10	0	2	0	10	1	8	0	0.6	0.4	0.1	0.2	0	0.7	7.4
NVa18-8	3	4	98	3130	4520	6	29	22	0	23	25	32	2	29	8	1	11	0.9	0.5	0.4	0.1	0.2	0	0.7	5.9
NVa18-9	34	4	176	2430	4180	308	72	39	0	34	20	317	5	14	17	2	22	0.6	1.1	1.3	0	0.4	0	1.6	24.9
NVa18-10	28	4	167	2620	4280	248	68	39	0	39	19	90	4	10	15	2	19	0	0.9	1.1	0	0.3	0	1.5	20.5
Nvb18-1	29	4	180	2390	3510	277	75	42	0	28	14	159	5	0	13	2	14	0	0.8	1	0	0.2	0	1.2	18.3
Nvb18-2	32	5	178	2350	3440	280	81	39	0	33	18	111	4	7	15	2	15	0	0.9	1.2	0.4	0.4	0	1.4	19.2
NVb18-3	19	4	119	2290	3540	98	61	25	0	22	19	43	3	0	10	2	10	0	0.6	0.7	0.2	0.2	0	1	8.2
NVb18-4	18	4	114	2430	3740	95	60	26	0	29	18	42	3	0	10	2	11	0	0.7	0.7	0.1	0.3	0	1	9
NVb18-5	25	3	242	1650	2480	166	69	49	0	32	22	199	6	13	19	2	21	0.7	1.2	0.8	0	0.4	0	1.8	14.9
NVb18-6	25	3	241	1710	2620	161	80	49	0	34	24	243	5	9	20	3	23	0.9	1.2	1	0.1	0.6	0	1.8	15.5
NV18-1	35	4	197	2130	3820	314	76	44	0	37	26	74	6	5	17	2	20	0	1.1	1.3	0	0.5	0	1.7	23.1
NV18-2	38	4	253	1720	3350	355	59	55	0	43	34	112	6	9	20	3	27	0.7	1.2	1	0	0.4	0	2	24.9
NV18-3	6	4	94	3160	4500	26	34	0	0	26	26	36	2	27	8	1	9	0.6	0.6	0.5	0.1	0.3	0	0.8	8
NV18-4	17	4	105	3100	4720	134	45	23	0	36	22	121	2	0	9	2	10	0	0.6	0.7	0.1	0.2	0	0.8	12.6
NV18-5	3	4	77	2960	4180	6	26	24	0	55	19	44	3	44	11	2	11	0.5	0.8	0.4	0.1	0.3	0	1	2.5
NV18-6	5	4	84	2960	4310	8	35	0	0	22	18	44	2	34	10	2	11	0.8	0.7	0.6	0.1	0.3	0	0.9	3.3
NV18-7	7	3	83	2510	3890	23	39	0	0	21	21	0	2	9	9	2	9	0.8	0.6	0.6	0.1	0.1	0	1.1	2.3
NV18-8	17	3	99	2100	3610	89	44	0	0	21	16	54	2	0	9	1	9	0	0.7	0.6	0.1	0.2	0	0.9	4.6
NV18-9	29	3	169	1830	3360	249	69	31	0	36	24	100	4	7	15	2	20	0	1	1.2	0	0.4	0	1.4	23.1
NV18-10	31	3	248	1570	2820	256	89	48	3	48	37	77	6	12	23	3	38	1.8	1.6	1.6	0	0.6	0	2.2	30.5
Shales																									
NV0.25	27	4	434	657	292	59	142	185	19	69	90	56	24	77	108	12	3	1.9	7.6	4.1	0.9	0.2	0	11.4	6.2
NV12.10	27	3	422	496	141	53	127	130	160	189	116	395	21	97	107	10	19	4.4	8.1	3.6	0.7	2.6	8	9.9	9.5
NV12.60	29	3	326	525	156	28	141	112	69	119	71	417	22	11	123	12	0	1.3	9.7	3.8	0.9	0.7	8	8.4	7.0
NV13.20	16	3	210	435	129	44	70	65	25	36	29	89	11	17	57	6	0	0.7	4.4	1.9	0.4	0.2	5	4.4	4.4

similar to those found in the coeval shales (Table 5). The low thorium/uranium ratios mainly reflect the very low thorium concentrations and high uranium values in the phosphates. This may be the combined result of minor quantities of heavy minerals (low Th) and reducing depositional concretionary conditions, characterized by high uranium and vanadium concentrations. Decreasing thorium/uranium ratios towards the rims of the concretions weakly indicate a gradual reduction in the oxygen level of the pore water (Table 5).

Table 4 Results of rare earth element analyses of phosphates and four typical shales from the Nordvik section.

Nordvik	La ppm	Ce ppm	Pr ppm	Nd ppm	Sm ppm	Eu ppm	Gd ppm	Tb ppm	Dy ppm	Ho ppm	Er ppm	Tm ppm	Yb ppm	Lu ppm
NV19-1	87.1	157	15.4	61.4	13.3	4	16.1	3	18.3	3.9	12.3	1.79	10.7	1.57
NV19-2	10.8	16.4	1.67	6.4	1.4	0.39	1.6	0.3	2.1	0.5	2	0.35	2.5	0.42
NV19-3	8.1	13	1.39	5.1	1.1	0.33	1.3	0.3	1.7	0.5	1.7	0.28	2	0.32
NV19-4	9.5	13.8	1.46	5.6	1.2	0.36	1.5	0.3	2	0.5	1.9	0.34	2.4	0.41
NV19-5	9.3	14.6	1.56	5.8	1.3	0.39	1.5	0.3	1.8	0.4	1.5	0.24	1.7	0.27
NV16-1	156	247	24.4	91	19.7	6.17	26.8	5	30.4	6.8	21.9	3.24	19.7	2.83
NV16-2	7.8	9.3	0.96	3.6	0.8	0.22	0.8	0.2	1.1	0.3	1.2	0.23	1.7	0.3
NV16-3	4	6.7	0.8	2.9	0.7	0.19	0.7	0.1	0.6	0.1	0.5	0.1	0.8	0.14
NV16-4	12.1	11.7	1.13	4.3	0.9	0.27	1.1	0.2	1.5	0.4	1.8	0.32	2.4	0.44
NV16-5	97.9	152	14.1	53.4	11.2	3.46	14.6	2.7	16.7	3.7	11.4	1.7	10.5	1.53
NV1740-1	191	258	25	96.3	21	6.5	28.1	5.3	34.5	8.1	26.7	4.24	27.6	4.19
NV1740-2	44.7	51.1	4.66	16.3	3.1	0.99	4.8	0.9	6.5	1.7	6.2	1.01	6.9	1.17
NV1740-3	3.9	5.7	0.63	2.4	0.5	0.15	0.5	0	0.6	0.2	0.7	0.14	1.2	0.22
NV1740-4	2.9	5.4	0.62	2.5	0.6	0.17	0.6	0	0.6	0.1	0.5	0.09	0.7	0.15
NV1740-5	106	151	13.8	51.6	11	3.32	13.8	2.7	17.2	4.1	14.2	2.29	14.9	2.32
NV33/17	152	231	23.6	88.6	18.5	5.36	22.5	4.2	24.8	5.4	17.7	2.63	16.4	2.4
NVa18-1	107	176	17	63.5	13.1	4.34	17.9	3.2	19.7	4.2	12.7	1.86	11.5	1.71
NVa18-2	112	178	17.3	64.5	13.2	4.29	17.8	3.3	20.3	4.4	13.1	1.87	11.6	1.72
NVa18-3	7.2	9.4	1.06	3.9	0.8	0.19	0.8	0.1	1	0.2	0.9	0.17	1.4	0.24
NVa18-4	14	14.7	1.44	5.1	1	0.32	1.3	0.3	1.9	0.5	1.9	0.35	2.7	0.48
NVa18-5	3.4	6.2	0.75	2.9	0.6	0.15	0.6	0.1	0.6	0.1	0.4	0.06	0.4	0.07
NVa18-6	2.8	5.4	0.68	2.7	0.5	0.13	0.5	0	0.5	0.1	0.3	0	0.4	0.07
NVa18-7	4.5	5.9	0.69	2.7	0.6	0.13	0.5	0	0.6	0.2	0.6	0.11	0.9	0.19
NVa18-8	3.1	5.6	0.69	2.7	0.5	0.11	0.5	0	0.5	0.1	0.4	0.06	0.5	0.1
NVa18-9	142	220	22.4	81.9	17	5.58	22.2	4.1	26.3	6.1	18.3	2.67	16	2.46
NVa18-10	108	162	16.2	59	12.6	4.04	16	3	19.4	4.5	13.7	2.01	12.6	1.97
Nvb18-1	121	187	19	69.3	14.7	4.8	19.1	3.4	22.5	5	15.5	2.3	13.8	2.06
Nvb18-2	133	207	20.9	75.6	16.2	5.27	20.7	3.8	25.1	5.6	16.7	2.45	14.8	2.23
NVb18-3	32	26.9	2.28	7.8	1.4	0.49	2.2	0.4	3.7	1.1	4.3	0.8	5.8	0.97
Nvb18-4	29.5	23.7	2.04	7.1	1.4	0.45	2	0.4	3.7	1.1	4.2	0.79	5.9	1.03
NVb18-5	92.8	156	15.4	57.7	11.7	3.72	14.6	2.6	17.1	3.6	10.5	1.48	9	1.36
NVb18-6	85.4	143	14	52.8	10.9	3.5	13.3	2.4	16	3.4	9.8	1.4	8.6	1.35
NV18-1	151	239	24.3	93	18.7	6.21	23.6	4.4	28.7	6.4	19	2.74	16.1	2.42
NV18-2	174	292	31.3	121	25.5	7.98	31.1	5.7	35.7	7.4	21.2	2.96	18	2.66
NV18-3	7.4	8.4	0.88	3.4	0.7	0.14	0.8	0.1	1.1	0.3	1.1	0.21	1.6	0.32
NV18-4	44	47.7	4.19	15.1	2.8	0.94	4.5	0.9	7	1.8	6.3	1.05	6.9	1.15
NV18-5	4.3	8.3	1.01	3.8	0.8	0.18	0.8	0.1	0.8	0.2	0.4	0.07	0.5	0.08
NV18-6	3.9	6.9	0.86	3.3	0.6	0.15	0.6	0.1	0.7	0.1	0.5	0.09	0.7	0.13
NV18-7	9.4	10.7	1.27	4.5	0.8	0.22	1	0.2	1.2	0.3	1.2	0.21	1.6	0.31
NV18-8	34.1	36.5	3.1	11.3	2.2	0.72	3.2	0.6	4.9	1.3	4.5	0.74	5.1	0.83
NV18-9	124	206	20.6	80	16.3	5.18	21	3.9	24.5	5.2	14.8	2.17	12.9	1.9
NV18-10	134	252	26.5	103	21.5	6.86	26.6	4.9	29.1	6	15.9	2.21	12.9	1.89
Shales														
NV0.25	61.7	116	12.8	46.4	9	2.47	8.7	1.5	8.8	1.7	4.7	0.69	4.4	0.66
NV12.10	53.2	110	11.9	44	8.6	2.47	9	1.5	8.2	1.6	4.5	0.64	4.1	0.66
NV12.60	33.1	70.8	7.29	25.6	4.9	1.34	4.5	0.8	4.5	0.9	2.7	0.4	2.6	0.43
NV13.20	31.3	62.5	6.66	25.9	5.5	1.62	6	1	5.9	1.2	3.3	0.47	3	0.47

Some clear-cut differences appear when element ratios from the Nordvik phosphate concretions and associated shales are compared. In both the Nordvik shales and concretions, the Al_2O_3 concentration is a measure of the general clastic content. The high Sc/Al_2O_3 values and their large variations are typical in the phosphates, showing relative scandium enrichments in the phosphates compared with the shales. Similar concretionary enrichments are also evident from Cu, Ba and Zn analysis, as seen in their very high Cu/Al_2O_3, Ba/Al_2O_3 and Zn/Al_2O_3 ratios. The lower K_2O/Al_2O_3 ratios in the phosphates may reflect a higher content of fine-grained

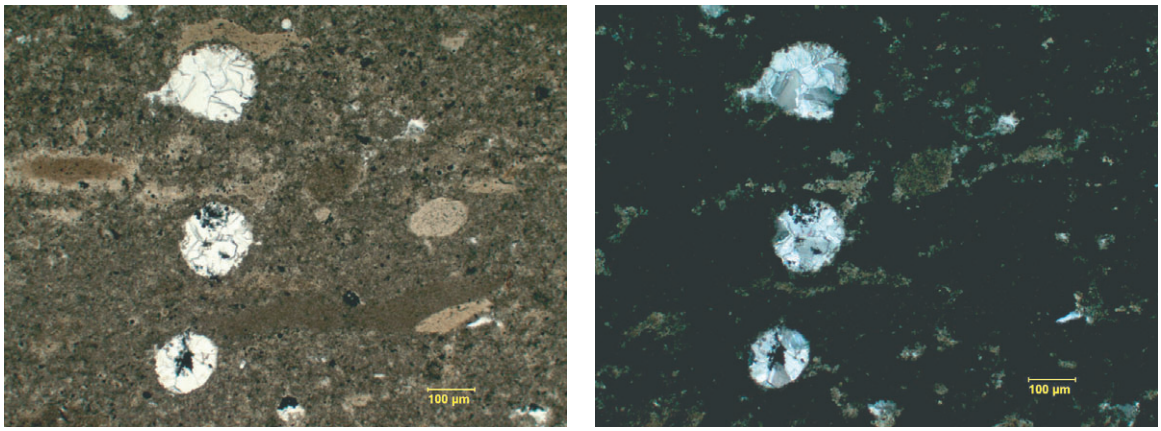

Fig. 5 Thin-section microphotographs of phosphate concretion NV18: to the left in ordinary light; to the right with crossed polarizers. Light-grey sparitic calcite fills the fossil tests, whereas fine-grained calcite and phosphate forms the major part of the peloidal brown (to the left) and dark-grey to black (to the right) parts of the micrographs.

kaolinitic clays compared with the more illitic and feldspar-rich shales, which display higher K_2O/Al_2O_3 ratios.

Comparison of REEs in shales and concretions. The REE patterns in the Nordvik shales and phosphates are very different (Fig. 7). The four shale samples analysed display moderate total REE enrichments compared with the standard upper continental crustal values (Condie 1991), with total REE concentrations between 154 and 279 ppm. In the phosphates the total REE content varies severely, from 14 to 736 ppm in the 42 samples analysed. Typically the inner parts of the phosphate concretions are low in total REEs and display very flat, normalized distribution patterns, whereas increasing enrichments in total REEs are found towards the concretionary rims. The phosphates are generally enriched in the HREE compared with the shales (Fig. 7).

In the different runs of correlation coefficient analyses no particular associations have appeared between the REEs and any particular mineral (mineral identification/quantification based on semi-quantitative XRD analyses), or major and minor elements. No clear-cut enrichments in the commonly studied LREE (La, Ce, Pr and Nd), middle rare earth element (MREEs: Sm, Eu, Gd and Tb) and HREE (Dy, Ho, Er, Tm, Yb and Lu) fractions were established.

REE variations within the phosphate concretions. The total REE enrichments along the margins are several orders of magnitude higher when compared with the central parts of the concretions, where normally the lowest concentrations occur. In most of the concretions no particular zonations in LREE/HREE ratios are found, being close to constant within the seven concretions studied.

High (up to four times) HREE enrichments are typical for modern ocean water, accompanied by cerium depletion (McArthur & Walsh 1984; Byrne & Sholkovitz 1996; Murthy et al. 2004). In the samples of this study no cerium anomaly has been observed. The HREE enrichments and lack of cerium depletion in the phosphates may reflect reducing bottom sea water conditions at the time of formation.

The developments of the REE rim enrichments can probably not be explained by siliciclastic contamination, as the surrounding Nordvik shales contain less total REEs than the enriched marginal phosphates. The high rim concentrations may be a diagenetic effect, with mutual REEs and uranium, vanadium and zinc enrichments in the very last phosphate-precipitating solutions.

Geochemical studies may illustrate possible mechanisms of phosphate formation at the anoxic/oxic boundary. The search for systematic REE fractionation within the analysed concretions has been negative, as has the search for distributional trends of possible cerium and europium anomalies. The presence of such anomalies could have been of great interest, reflecting varying redox conditions (Ce) or extreme concentrations of feldspar (Eu) (Byrne & Sholkovitz 1996; Murthy et al. 2004). The europium anomalies calculated for these phosphates are normally above 1. A couple of very low values are found in the rather pure apatite samples of NVa18-8 and NV18-3. These two samples were taken from the inner part of the concretions, but not from the very centre. They represent the only low values found in the seven concretions studied, and could characterize the redox

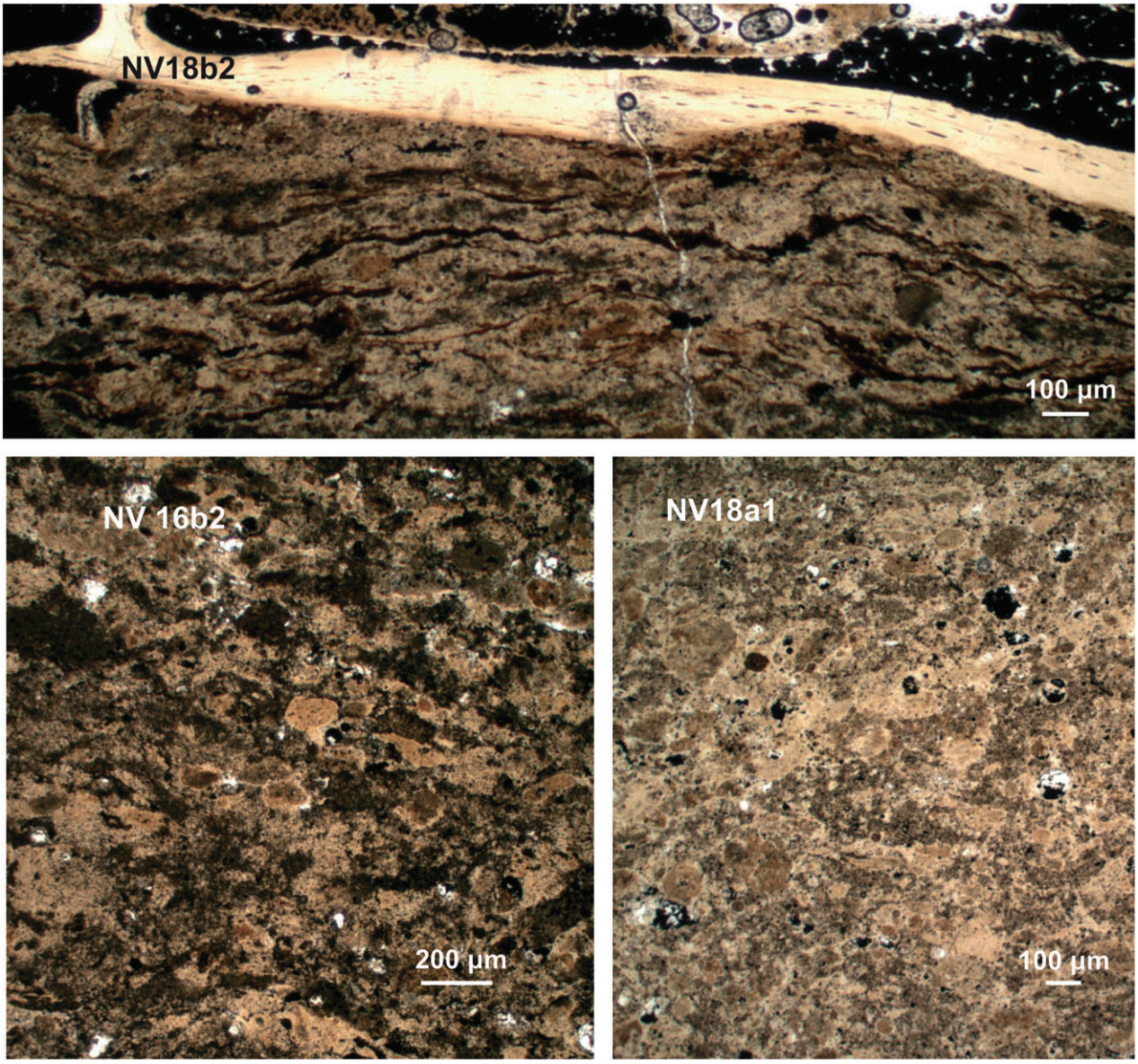

Fig. 6 Thin-section microphotographs of phosphate concretions NV18 and NV16. The upper micrograph (sample NV18b2) displays a bone fragment covered by black, framboidal pyrite along the upper side, whereas possible algal lamination is present in the lower half of the micrograph. The lower two micrographs display the peloidal texture typically found in the concretions. Algal remnants are displayed as dark spots in the lower left micrograph (sample NV16b2).

variations in an early stage of concretionary formation. Kidder et al. (2003) found europium anomalies in phosphate concretions reflected extreme reducing conditions. An explanation of the europium anomaly related to higher quantities of clastic feldspar content seems less likely, and is not compatible with the very low feldspar quantities detected in the XRD analyses.

The cerium-anomaly variations are very subtle, with average values just above 1, reflecting only weakly oxidizing conditions in the water masses (Murthy et al. 2004). Cerium may precipitate from seawater, and phosphates are generally poor in cerium. No correlation has been found between cerium and any particular minerals or elements other than the REEs. The faint indications of somewhat lower cerium concentrations in the central parts of the concretions indicate poor oxidizing conditions in the bottom waters or early pore fluids present in the early phases of phosphate precipitation.

The different phosphate concretions display comparable REE compositions. The NV19 concretion is the only one

Table 5 Geochemical ratios from the concretions and four typical shales analysed (raw data from Tables 1 and 3).

Samples	Sc/Al_2O_3	K_2O/Al_2O_3	Ba/Al_2O_3	Cu/Al_2O_3	Zn/Al_2O_3	V/Cr	V/Cu	Cr/Cu	Mo/Cu	Mo/Zn	Cu/Zn	Th/U
NV19-1	6.93	0.14	1218.98	8.76	33.21	3.63	6.04	1.67	0.00	0.00	0.26	0.13
NV19-2	5.48	0.15	1433.79	8.68	17.35	4.70	7.42	1.58	0.00	0.00	0.50	0.33
NV19-3	3.35	0.13	624.54	5.20	0.00	6.79	16.50	2.43	0.00	1.00	1.00	0.60
NV19-4	5.64	0.17	1953.85	8.72	31.79	3.75	7.06	1.88	0.00	0.00	0.27	0.30
NV19-5	2.94	0.16	1578.43	10.29	42.65	3.83	5.48	1.43	0.10	0.02	0.24	0.19
NV16-1	11.86	0.13	733.97	5.13	29.81	5.59	11.88	2.13	0.94	0.16	0.17	0.07
NV16-2	0.35	0.01	150.29	0.69	1.79	3.65	7.00	1.92	0.67	0.26	0.39	0.12
NV16-3	3.10	0.16	2209.30	8.53	35.66	10.00	7.36	0.00	0.82	0.20	0.24	0.19
NV16-4	6.72	0.12	2044.78	8.96	50.00	10.00	7.33	0.00	0.75	0.13	0.18	0.24
NV16-5	9.39	0.13	732.85	5.42	44.04	5.19	12.47	2.40	0.93	0.11	0.12	0.09
NV1740-1	20.67	0.10	690.00	8.00	187.00	5.79	10.13	1.75	0.50	0.02	0.04	0.03
NV1740-2	15.63	0.06	2156.25	10.16	121.09	6.59	11.15	1.69	0.69	0.06	0.08	0.20
NV1740-3	5.15	0.12	1669.12	9.56	38.24	10.00	10.62	0.00	0.46	0.12	0.25	0.21
NV1740-4	4.10	0.08	1745.90	12.30	65.57	10.00	9.07	0.00	0.47	0.09	0.19	0.24
NV1740-5	20.12	0.14	1579.27	8.54	229.27	5.85	11.29	1.93	0.57	0.02	0.04	0.06
NV33/17	9.21	0.14	621.05	5.53	33.42	4.25	10.33	2.43	0.19	0.03	0.17	0.14
NVa18-1	10.00	0.13	621.43	5.36	27.50	4.02	12.07	3.00	1.33	0.26	0.19	0.07
NVa18-2	10.74	0.12	696.30	5.93	68.52	4.18	11.50	2.75	1.19	0.10	0.09	0.07
NVa18-3	4.19	0.14	1508.98	7.19	27.54	3.63	7.25	2.00	0.75	0.20	0.26	0.48
NVa18-4	7.10	0.14	1331.36	0.00	55.62	3.77	20.00	3.00	2.00	0.13	0.00	0.37
NVa18-5	2.56	0.16	1452.99	0.00	0.00	10.00	20.00	3.00	2.00	1.00	1.00	0.24
NVa18-6	2.61	0.12	2252.17	8.70	51.30	10.00	7.50	0.00	1.00	0.17	0.17	0.35
NVa18-7	3.88	0.12	2224.81	7.75	0.00	4.13	9.50	2.30	0.80	1.00	1.00	0.09
NVa18-8	2.52	0.17	2630.25	21.01	26.89	4.45	3.92	0.88	0.44	0.34	0.78	0.12
NVa18-9	11.53	0.14	823.73	6.78	107.46	4.51	8.80	1.95	1.10	0.07	0.06	0.06
NVa18-10	10.73	0.13	1003.83	7.28	34.48	4.28	8.79	2.05	1.00	0.21	0.21	0.07
Nvb18-1	11.33	0.13	933.59	5.47	62.11	4.29	12.86	3.00	1.00	0.09	0.09	0.07
Nvb18-2	11.68	0.12	857.66	6.57	40.51	4.56	9.89	2.17	0.83	0.14	0.16	0.07
NVb18-3	11.24	0.13	1355.03	11.24	25.44	4.76	6.26	1.32	0.53	0.23	0.44	0.12
NVb18-4	11.32	0.13	1528.30	11.32	26.42	4.38	6.33	1.44	0.61	0.26	0.43	0.11
NVb18-5	6.94	0.12	458.33	6.11	55.28	4.94	11.00	2.23	0.95	0.11	0.11	0.12
NVb18-6	7.12	0.12	487.18	6.84	69.23	4.92	10.04	2.04	0.96	0.09	0.10	0.12
NV18-1	7.69	0.09	468.13	5.71	16.26	4.48	7.58	1.69	0.77	0.27	0.35	0.07
NV18-2	8.90	0.12	402.81	7.96	26.23	4.60	7.44	1.62	0.79	0.24	0.30	0.08
NV18-3	4.58	0.16	2412.21	19.85	27.48	10.00	3.62	0.00	0.35	0.25	0.72	0.10
NV18-4	11.64	0.14	2123.29	15.07	82.88	4.57	4.77	1.05	0.45	0.08	0.18	0.06
NV18-5	1.61	0.11	1591.40	10.22	23.66	3.21	4.05	1.26	0.58	0.25	0.43	0.40
NV18-6	3.31	0.17	1960.26	11.92	29.14	10.00	4.67	0.00	0.61	0.25	0.41	0.27
NV18-7	5.30	0.14	1901.52	15.91	0.00	10.00	3.95	0.00	0.43	1.00	1.00	0.48
NV18-8	10.37	0.15	1280.49	9.76	32.93	10.00	6.19	0.00	0.56	0.17	0.30	0.20
NV18-9	10.82	0.12	682.84	8.96	37.31	5.45	7.04	1.29	0.83	0.20	0.24	0.06
NV18-10	7.40	0.13	374.70	8.83	18.38	5.17	6.70	1.30	1.03	0.49	0.48	0.07
Shales												
NV0.25	1.46	0.14	35.51	4.86	3.03	2.35	4.82	2.06	0.03	0.05	1.61	1.78
NV12.10	1.69	0.16	30.96	7.24	24.66	3.25	3.64	1.12	0.16	0.05	0.29	1.04
NV12.60	1.54	0.16	27.91	3.77	22.17	2.91	4.59	1.58	0.00	0.00	0.17	1.20
NV13.20	1.88	0.17	51.24	3.42	10.48	3.23	7.24	2.24	0.00	0.00	0.33	1.00

showing some deviation, with reduced quantities of LREEs than the other concretions. This may reflect relatively lower calcite and higher apatite contents. In the phosphates, iridium and platinum-group elements enrichments were expected, as presented earlier by Zakharov et al. (1993) in other samples of the same Nordvik beds. The phosphates clearly represent periods and sites of confined clastic sedimentation, with a high preservation potential for any extraterrestrial cosmic influx, possibly suffering some alterations below the water–sediment interface. In this project we have also analysed iridium levels, but no high enrichments were found. Dr F.T. Kyte analysed the samples and found no values above 200 ppt (F.T. Kyte, pers. comm., 2006).

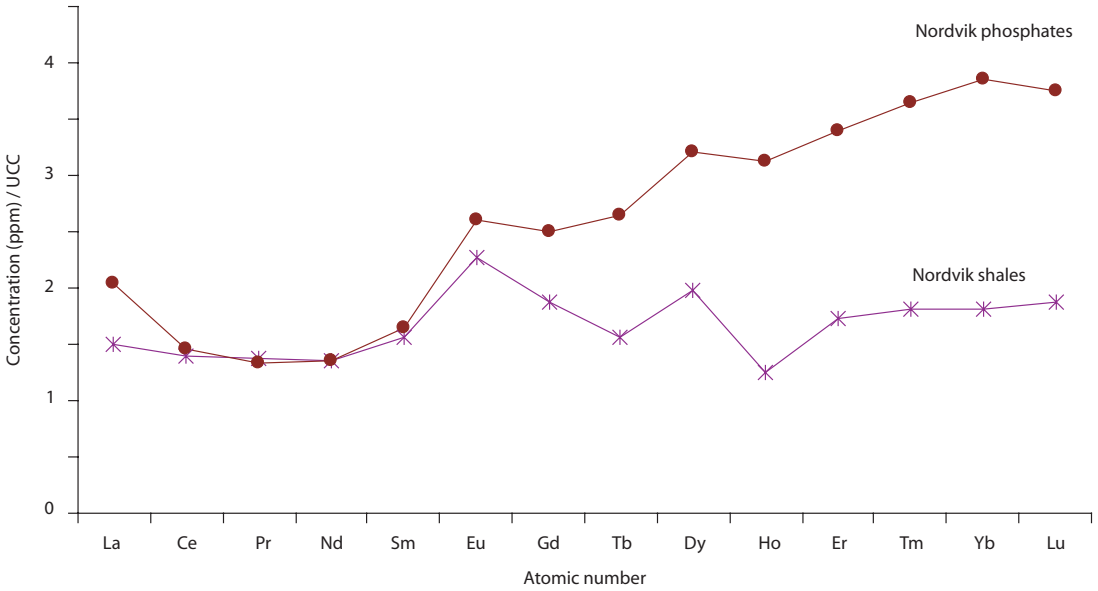

Fig. 7 Normalized (average upper continental crust values [UCC]; see Condie [1991]) rare earth element (REE) distribution of average values of Nordvik shales and phosphates. The shales, and in particular the phosphates, display relative enrichments in the heavy REEs. The REEs are plotted according to increasing atomic number.

Zakharov et al. (1993) reported iridium enrichments of up to 7 ppb in the Nordvik area, but only in a very thin zone, which we were not able to detect in the present study.

Discussion of stratigraphical and regional trends

The mineralogical and geochemical analyses display distributional associations as expected from the correlations, i.e., components related to clay minerals, heavy minerals and siliciclastics are enriched in the shales, whereas elements related to phosphates and carbonates are enriched in the concretions. At lower latitudes phosphates have often been shown to suffer from geochemical alterations as a result of weathering (Perkins & Foster 2004; Herring & Grauch 2004). In Nordvik, this is only a minor problem, a possible result of its rather recent High-Arctic exposure under extreme dry and cold conditions. Murthy et al. (2004) claimed MREEs to be distally enriched in the depositional basin as a result of MREE co-precipitation with phosphates. In our study we have not observed any MREE enrichments, and the lanthanum concentrations are much more varied and higher compared with those of Murthy et al. (2004).

In thin-section inspections the phosphorites are seen to contain small quantities of algae and to be rich in fossils, even carrying remnants of bones (Fig. 6). They normally resemble the pristine phosphates of the Triassic Bravaisberget and Botneheia formations in Svalbard (Krajewski 2000a). Their organic content represents an important source of phosphate in addition to the supply from a possible external source through the diagenetic, bacterial breakdown of organic matter. The geochemical relations of, for example, the concentrations of vanadium, copper, zinc and cadmium indicate a microbiological origin for the phosphorites (cf. Perkins & Piper 2004). The Nordvik concretions have low K_2O/Al_2O_3 ratios compared with the adjacent shales, maybe mirroring a higher content of fine-grained, clastic kaolinite in the phosphorites than in the adjacent shales. It is most likely a clastic kaolinite; so far no diagenetic kaolinite has been found in the SEM analysis. The concretions contain traces of sphalerite and pyrite, and are mainly found to be composed of fluor (or hydroxy) apatite. Higher vanadium concentrations in the phosphates than in the accompanying shales, along with the sulphide variations and uranium enrichments (low Th/U ratios) indicate partly reducing to dysoxic, early diagenetic conditions. This is in some contrast to the weak cerium anomaly. In the Bazhenov Formation to the west, good correlation between the natural gamma radioactivity (in particular U, Th and K_2O) and the level of TOC is common (Gavshin & Zakharov 1996a, b). The enrichments in total REEs and vanadium, and low thorium/uranium ratios, and high Cu/Al_2O_3 and Zn/Al_2O_3 ratios along the outer rim may demonstrate their formation mechanism, indicating more reducing conditions in their late phases of growth. The phosphates display low thorium/uranium ratios compared with the Nordvik shales, underlining the partly dysoxic depositional

conditions (low thorium and relatively high uranium concentrations). Well-developed parallel lamination and confined bioturbation also shows limited oxygen contents and reduced benthic life.

In particular, high Sc/Al_2O_3 ratios are found in the phosphates. High scandium concentrations are typically found in basaltic material (Taylor 1965), in this case probably reflecting a possible input of basaltic Siberian traps material into the Siberian Basin.

Formation of phosphates: general setting

The late Jurassic setting of the Arctic Siberian platform was a wide, low relief area with dominant sediment supply of fine-grained clays and well-weathered sediments and volcanics (Siberian traps). In contrast, the marginal deposits of, for example, Greenland, Svalbard and the western Barents Sea were siltier, located closer to regional clastic sedimentary source areas, and partly influenced by the large-scaled tectonics of the incipient opening of the Arctic Ocean (Lawver et al. 1990; Dypvik et al. 2002; Dypvik et al. 2006). Reduced clastic sedimentation of fine-grained material dominated the Nordvik conditions, with relatively high organic production, maybe related to upwelling current effects in the rather shallow epicontinental Arctic. This illustrates the major difference between the western and eastern Arctic localities studied, and can explain why phosphates at this time were deposited in Siberia and not in the western Arctic. The transgressive late Jurassic phase resulted in an overall reduced clastic input and increased organic production in the low-lying areas. Arctic upwelling has been, and still is, up for discussion (Buckley et al. 1979; Parrish et al. 2001; Khain & Filatova 2007).

The phosphate precipitation took place along the sea floor, a few centimetres below the sea bed, possibly in anoxic to dysoxic conditions. The bacterial breakdown of algal-rich organic matter, which probably liberated phosphates, could have been produced in the Siberian region by a possible upwelling from deeper water locations to the north-west. This mechanism of early diagenetic precipitation may be comparable with what Bremner & Rogers (1990), Burnett (1990), and Burnett & Riggs (1990) and others described from Peruvian localities, with the general oceanographic setting excepted. There, phosphate precipitation occurred as crusts about 2 cm thick, 10–20 cm deep in the sediments. The phosphate was released in the sediments by bacterial degradation of organic matter and precipitated as apatite in the pore space. Based on the first palaeo-oceanographic calculations (Haupt et al., unpubl. ms), late Jurassic upwelling conditions seem possible along the Siberian margin, but the palaeo-water depth was shallow and the bathymetric relief was subdued.

In the Nordvik phosphates vertebrate bones are present and peloidal textures and possible algal structures have been seen in the thin sections (Fig. 6). The main algal-related explanation (see above) would also fit the geochemical characteristics found (high V, Cu, Zn and Cd concentrations). Algal structures have also been observed macroscopically in the time-equivalent Bazhenov Formation of west Siberia (Filina et al. 1984).

Phosphate-rich pore waters promote phosphate precipitation (Glenn 1990), which may happen on the upper continental slope, where the O_2-minimum layer impinges the slope, the sea-floor sediments are high in organic-rich muds, and bacterial activity is present (Reimers et al. 1990; Glenn & Arthur 1988). The fine-laminated phosphatic, algal mats are found at the oxic–anoxic transition, in an area with organic-rich shales. This may also have been the case for the Siberian phosphates. The lack of dolomite in the Siberian phosphorites is, however, in some contrast to the common phosphates and dolomite association found, for example, in Peruvian phosphorites (Glenn & Arthur 1988).

Krajewski (2000a, b, c, d) has studied in great detail the Triassic phosphate concretions of Svalbard (Bravaisberget/Botneheia formations). The Paksa Formation phosphorites can be compared with the so-called pristine phosphates of Krajewski (2000a), which also lack reworking. In the Paksa Formation the conditions of phosphate formation may have changed through time, as was the case in the Triassic of Svalbard (Bravaisberget/Botneheia formations) (Krajewski 2000b). In both cases the main phosphate precipitation took place within partly mat-stabilized sediments, in a narrow zone near the anoxic–oxic interface. In the Triassic of Svalbard case (Krajewski 2000b) the phosphate precipitation occurred just above the sulphate reduction zone.

In the Meade Peak Member, Perkins & Piper (2004) analysed the Cd/Zn, Mo/Zn, Cd/Cu and Mo/Cu ratios, which they found to be rather similar to modern plankton. They therefore claimed an original biogenic phosphate source. In the Siberian phosphates traces of algal material have been observed in the thin sections (Fig. 6), and comparable geochemical ratios have been established (Martin & Knauer 1973; Collier & Edmond 1984). Some minor geochemical excursions in the phosphates may result from the varying contents of clastic components, e.g., more terrigeneous material along the margins, compared with those from central basinal locations. Phytoplanktonic rain brought the organic matter to the sea floor from the photic zone. Most likely via bacterial oxidation near the oxic–anoxic transition, probably just above the oxic–anoxic interface, the phosphate was released to the pore water, eventually resulting in phosphate precipitation within the very finely laminated beds.

The phosphate composition during precipitation was in continuous change, as reflected in the geochemical composition.

In the Siberian phosphates weak positive cerium anomalies occur in flat, normalized REE patterns. The outer parts of the concretions are enriched in total REEs, along with uranium, vanadium, rubidium and scandium, possibly reflecting diagenetic phases in the later part of concretionary formation with reducing conditions in the enriched precipitating pore water. Maximum REE values in marine water are typically found where major sulphate reduction happens; consequently, minor quantities are normally to be expected in the clastic sediments (de Baar et al. 1988; Sholkovitz et al. 1994).

In the literature, outer parts of concretions commonly display low Th/U ratios, and enrichments in zinc and REEs, comparable with the Siberian concretions studied, a possible reflection of diagenetic phosphate growth just below the sea floor, e.g., comparable with the Phosphoria Formation (Hein et al. 2004) and Namibian shelf occurrences (Baturin 2000). In the Siberian concretions dark, possibly diagenetic, zones have been discovered in the thin sections. These zones commonly cut across the parallel lamination of the concretions. We have, in detail, analysed and searched these black-coated regions, but so far we have not been able to detect their composition. It looks like a thin varnish of manganese ferric oxides, but the compositional difference with the surrounding was too small to be detected in our geochemical, SEM or microprobe analyses. The black zones could represent organic matter or sulphides. In the SEM runs sphalerite (ZnS) has shown up in parts of the phosphates. This may, in combination with some very finely distributed organic matter, form the dark areas.

Conclusion

The deposition of fine-grained, well-weathered, clastic sedimentary particles took place through highly productive, oxygen-rich upper water masses, before final deposition in mainly dysoxic depositional environments along the shallow, epicontinental sea floor. Dark, organic-rich clays and claystones were the common sediments, interrupted by quieter periods with high organic production and diagenetic phosphate concretion formation.

In the Nordvik area, the most fine-grained sedimentation happened in combination with high organic production/sedimentation, high algal production and possibly upwelling. These conditions resulted in well-developed phosphate precipitation, confined to thin, laminated beds dispersed in the succession. The phosphate concretions reflect the simultaneously reduced clastic sedimentation and succeeding diagenesis in shelf environments during the prevailing oxygen-deficient conditions along the sea floor. In the Barents Sea region to the west of Nordvik, periods with reduced clastic accumulation are represented by thin carbonate beds of calcite, dolomite or siderite. In the Nordvik beds studied only weak signs of the Mjølnir impact have been found as faint iridium enrichments (about 200 ppt).

Acknowledgements

The comments of A. Mørk and two anonymous referees on earlier versions of the manuscript are highly appreciated. IKU/SINTEF Petroleum Research kindly made the core available and the late Øystein How is thanked for valuable assistance in the core laboratory at Dora (Trondheim).

References

Baturin G.N. 2000. Formation and evolution of phosphorite grains and nodules on the Namibian shelf, from recent to Pleistocene. In C.R. Glenn et al. (eds.): *Marine authigenesis: from global to microbial*. Pp. 185–199. Tulsa: Society for Sedimentary Geology.

Bremner J.M. & Rogers J. 1990. Phosphorite deposits on the Namibian continental shelf. In W.C. Burnett & S.R. Riggs (eds.): *Phosphate deposits of the world. Vol. 3. Neogene to modern phosphates*. Pp. 46–61. Cambridge: Cambridge University Press.

Buckley J.R., Gammelsrød T., Johannessen J.A., Johannessen O.M. & Røed L.P. 1979. Upwelling: oceanic structure at the edge of the Arctic ice pack in winter. *Science 203*, 165–167.

Burnett W.C. 1990. Phosphorite growth and sediment dynamics in the modern Peru shelf upwelling system. In W.C. Burnett & S.R. Riggs (eds.): *Phosphate deposits of the world. Vol. 3. Neogene to modern phosphates*. Pp. 62–72. Cambridge: Cambridge University Press.

Burnett W.C. & Riggs S.R. 1990. *Phosphate deposits of the world. Vol. 3. Neogene to modern phosphates*. Cambridge: Cambridge University Press.

Byrne R.H. & Sholkovitz E.R. 1996. Marine chemistry and geochemistry of the Lanthanides. In K.A. Schneider Jr. et al. (eds.): *Handbook on the physics and chemistry of rare earths. Vol. 23*. Pp. 497–595. Amsterdam: Elsevier.

Carroll D. 1970. *Clay minerals: a guide to their X-ray identification*. Boulder, CO: Geological Society of America.

Collier R.W. & Edmond J.M. 1984. The trace element chemistry of marine biogenic particulate matter. *Progress in Oceanography 13*, 113–199.

Condie K.C. 1991. Another look at rare-earth elements. *Geochimica et Cosmochimica Acta 55*, 2527–2531.

de Baar H.J.W., German C.R., Elderfield H. & van Gaans P. 1988: *Rare earth element distributions in anoxic waters of the Cariaco Trench. Geochimica et Cosmochimica Acta 52*, 1203–1219.

Dypvik H., Gudlaugsson S.T., Tsikalas F., Attrep M. Jr., Ferrell R.E. Jr., Krinsley D.H., Mørk A., Faleide J.I. & Nagy J. 1996. The Mjølnir structure—an impact crater in the Barents Sea. *Geology 24*, 779–782.

Dypvik H., Håkansson E. & Heinberg C. 2002. Jurassic and Cretaceous palaeogeography and stratigraphic comparison in the North Greenland–Svalbard region. *Polar Research 21*, 91–108.

Dypvik H., Smelror S., Sandbakken P.T., Salvigsen O. & Kalleson E. 2006. Traces of the marine Mjølnir impact event. *Palaeogeography, Palaeoclimatology, Palaeoecology 24*, 621–636.

Filina S.I., Korž M.V. & Zonn M.S. 1984. *Paleogeografija i neftenosnost' Baženovskoj Svity Zapadnoj Sibiri. (Palaeogeography and petroleum potental of the western Siberia Bazhenov Formation.)* Moscow: Nauka.

Gavshin V.M. & Zakharov V.A. 1996a. Bazhenovites on the Norwegian continental shelf. *Soviet Geology and Geophysics 32*, 52–59.

Gavshin V.M. & Zakharov V.A. 1996b. Geochemistry of the Upper Jurassic–Lower Cretaceous Bazhenov Formation, west Siberia. *Economic Geology 91*, 122–123.

Glenn C.R. 1990: Pore water, petrologic and stable carbon isotopi data bearing on the origin of Modern Peru margin phosphorites and associated authigenic phases. In W.C. Burnett & S.R. Riggs (eds.): *Phosphate deposits of the world. Vol. 3. Neogene to modern phosphates*. Pp. 46–61. Cambridge: Cambridge University Press.

Glenn C.R. & Arthur M. 1988: Petrology and major element geochemistry of Peru margin phosphorites and associated diagenetic minerals: authigenesis in modern organic-rich sediments. *Marine Geology 80*, 231–267.

Guldbrandsen R.A. 1970. *Relation of carbon dioxide content of apatite of the Phosphoria Formation to regional facies. US Geological Survey Professional Paper 700 B*. Washington, D.C.: US Geological Survey.

Hein J.R., Perkins R.B. & McIntyre B.R. 2004. Evolution of thought concerning the origin of the Phosphoria Formation, Western US Phosphate Field. In J.R. Hein (ed.): *Life cycle of the Phosphoria Formation: from deposition to post-mining environment. Handbook of geochemistry. Vol. 8*. Pp. 19–42. Amesterdam: Elsevier.

Herring J.R. & Grauch R.I. 2004. Lithogeochemistry of the Meade Peak Phosphatic Shale Member of the Phosphoria Formation, southeast Idaho. In J.R. Hein (ed.): *Life cycle of the Phosphoria Formation: from deposition to post-mining environment. Handbook of geochemistry. Vol. 8*. Pp. 321–366. Amesterdam: Elsevier.

Khain V.E. & Filatova N.I. 2007. Main stages in tectonic evolution of the Eastern Arctic region. *Doklady Earth Sciences 415*, 518–523.

Kidder D.L., Krishnaswamy R. & Mapes R.H. 2003. Elemental mobility in phosphatic shales during concretion growth and implications for provenance analysis. *Chemical Geology 198*, 335–353.

Krajewski K.P. 2000a. Phosphogenic facies and processes in the Triassic of Svalbard. *Studia Geologica Polonica 116*, 7–84.

Krajewski K.P. 2000b. Isotopic composition of apatite-bound sulphur in the Triassic phosphogenic facies in Svalbard. *Studia geologica Polonica 116*, 85–110.

Krajewski K.P. 2000c. Phosphorous concentration and organic carbon preservation in the Blanknuten Memember (Botneheia Formation, Middle Triassic), Sassenfjorden, Spitsbergen. *Studia Geologica Polonica 116*, 139–173.

Krajewski K.P. 2000d. Diagenetic recrystallization and neoformation of apatite in the Triassic phosphogenic facies in Svalbard. *Studia geologica Polonica 116*, 111–137.

Lawver L.A., Müller R.D., Srivastava S.P. & Roest W. 1990. In U. Bleil & J. Thiede (eds.): *The opening of the Arctic Ocean. Geological history of the Polar Ocean*. Pp. 29–62. Dordrecht: Klüwer Academic Publishers.

Martin J.H. & Knauer G.A. 1973. The elemental composition of plankton. *Geochimica et Cosmochimica Acta 37*, 1639–1653.

McArthur J.M. & Walsh J.N. 1984. Rare-earth geochemistry of phosphorites. *Chemical Geology 47*, 191–220.

McClellan G.H. & Lehr J.R. 1969. Crystal chemical investigation of natural apatites. *American Mineralogist 54*, 1374–1391.

Murthy R., Kidder D., Mapes R. & Hannigan R. 2004. Rare-earth element chemistry of Mississippian-age phosphate nodules in the Fayetteville Shale of Oklahoma and Arkansas. *Environmental Geosciences 11*, 99–111.

Parrish J.T., Droser M.L. & Bottjer D.J. 2001. A Triassic upwelling zone: the Shublik Formation, Arctic Alaska, U.S.A. *Journal of Sedimentary Research 71*, 272–285.

Perkins R.B. & Foster A.L. 2004. Mineral affinities and distribution of selenium and other trace elements in black shale and phosphorites of the Phosphoria Formation. In J.R. Hein (ed.): *Life cycle of the Phosphoria Formation: from deposition to post-mining environment. Handbook of geochemistry. Vol. 8*. Pp. 251–295. Amesterdam: Elsevier.

Perkins R.B. & Piper D.Z. 2004. The Meade Peak Member of the Phosphoria Formation: temporal and spatial variations in sediment geochemistry. In J.R. Hein (ed.): *Life cycle of the Phosphoria Formation: from deposition to post-mining environment. Handbook of geochemistry. Vol. 8*. Pp. 73–110. Amesterdam: Elsevier.

Reimers C.E., Kastner M. & Garrison R.E. 1990. The role of bacterial mats in phosphate mineralization with particular reference to the Monterey Formation. In W.C. Burnett & S.R. Riggs (eds.): *Phosphate deposits of the world. Vol. 3. Neogene to modern phosphates*. Pp. 300–311. Cambridge: Cambridge University Press.

Sholkovitz E.R., Landing W.M. & Lewis B.L. 1994. Ocean particle chemistry; the fractionation of rare earth elements between suspended particles and seawater. *Geochimica et Cosmochimica Acta 58*, 1567–1579.

Taylor S.R., 1965. The application of trace element data to problems in petrology. In L.H. Ahrens et al. (eds.): *Physics and chemistry of the Earth. Vol. 6*. Pp. 133–214. Oxford: Pergamon Press.

Zakharov V.A., Lapukhov A.S. & Shenfil O.V. 1993. Iridium anomaly at the Jurassic–Cretaceous boundary in northern Siberia. *Russian Journal of Geology and Geophysics 34*, 83–90.